Theoretical analysis and coating thickness determination of a dual layer metal coated FBG sensor for sensitivity enhancement at cryogenic temperatures

To cite this article: Rajinikumar Ramalingam and M D Atrey 2017 *IOP Conf. Ser.: Mater. Sci. Eng.* **278** 012075

IOP Conf. Series: Materials Science and Engineering **278** (2017) 012075 doi:10.1088/1757-899X/278/1/012075

Theoretical analysis and coating thickness determination of a dual layer metal coated FBG sensor for sensitivity enhancement at cryogenic temperatures

Rajinikumar Ramalingam[1,2] and M D Atrey[3]

[1] Institute of Technical Physics, Karlsruhe Institute of technology, Eggenstein-Leopoldshafen, 76344 Germany
[2] School of computing and Electrical Engineering, Indian Institute of Technology Mandi, 175005 Himachal Pradesh, India
[3] Department of Mechanical Engineering, Indian Institute of Technology Bombay, 400076, Maharashtra, India.

rajinikumar@iitmandi.ac.in

Abstract. Use of Fiber Bragg Grating (FBG) sensor is very appealing for sensing low temperature and strain in superconducting magnets because of their miniature size and the possibility of accommodating many sensors in a single fiber. The main drawback is their low intrinsic thermal sensitivity at low temperatures below 120 K. Approaching cryogenic temperatures, temperature changes lower than a few degrees Kelvin cannot be resolved, since they do not cause an appreciable shift of the wavelength diffracted by a bare FBG sensor. To improve the thermal sensitivity and thermal inertia below 77 K, the Bare FBG (BFBG) sensor can be coated with high thermal expansion coefficient materials. In this work, different metal were considered for coating the FBG sensor. For theoretical investigation, a double layered circular thick wall tube model has been considered to study the effect on sensitivity due to the mechanical properties like Young`s modulus, Thermal expansion coefficient, Poisson's ratio of selected materials at a various cryogenic temperatures. The primary and the secondary coating thickness for a dual layer metal coated FBG sensor have been determined from the above study. The sensor was then fabricated and tested at cryogenic temperature range from 4- 300 K. The cryogenic temperature characteristics of the tested sensors are reported.

1. Introduction

Selection of right sensors and an appropriate measurement system has become a challenging task as the operational requirements of the new technologies demands to measure extreme temperatures and conditions. The physical properties of the sensing material can change drastically in extreme temperatures. In the most advanced research centers, such as those using large particle accelerators [1], where cryogenic temperatures are essential for the proper operation of sensitive equipment, sensors capable of operating in these temperature ranges are essential. They serve to monitor both the conditions of a complex set of equipments required to perform the experiments, and to ensure the safety of the equipment itself. In order to fulfil the increasing demand for suitable cryo temperature sensors needed in advanced applications like ITER, KATRIN [2], HTS Geno [3] , the researchers look into the optical fiber sensors, which show distinctive advantages like immunity to electromagnetic interference and power fluctuations along the optical path, high precision, durability, compact size, ease of multiplexing a large number of sensors along a single fiber, resistance to corrosion and reduced cable dimensions [4-

7]. Among many optical fiber sensing techniques, Fiber Bragg Grating (FBGs) has become very prominent sensing method for many applications [8 – 12] and are being increasingly accepted by engineers, as they are particularly attractive to perform strain and temperature measurements under harsh environment areas, where conventional sensors cannot operate [13].

Moreover, the fact that it is stimulated by light signal minimizes the power dissipation in the sample while offering accuracy well suited to most applications. The response time is potentially low given the smaller sensor-size. Also the conditioning of the spectral signal can be easily processed with commercially available equipment. These capabilities make this type of sensors a preferable solution for monitoring environments where high electromagnetic fields are needed, such as those associated with monitoring of infrastructures used in superconducting magnets. Many groups are actively involved in designing and fabricating FBG sensors and studying its thermal characteristcis. It was shown experimentally that the Bragg wavelength of fused silica fibers with Germanium doped core becomes independent of temperature below 120 K. This is beneficial for structural health monitoring (strain) in cryogenic systems. On the other hand, bare fibers with FBG cannot be used for temperature measurements below 120 K. To overcome this problem, several solutions were proposed. Fixing the FBG on a substrate that shows a high thermal expansion such as polymer [14], flint-glass [15] or metals [16] result in a temperature dependence of several pm/K. Alternatively, metal-coating [17] of the fibers also lead to a measurable temperature dependence of the Bragg wavelength with minimal time lag. Proper selection of coating materials, coating dimensions and the coating techniques determine the performance and characteristic of a metal coated optical cryo sensor. The core of the sensor, in its original available form is covered with fiber cladding and with protective coating. In order to coat the bare sensors with chosen material this original cladding and protective coating have to be removed first. The thickness of the new coating determines induced thermal stresses acting on this “recoated” FBG sensor. However, larger coating thickness leads to thermal inertia. The thinner coating, on the other hand, has less thermal inertia but less sensitivity. Hence, it is essential to determine the correct coating thickness for given application for improving the performance of the sensor. In this paper, a theoritical model of dual metal coated FBG sensors were studied to determine the primary and secondary coating thickensses. The sensor was then fabricated and tested at cryogenic temperature range from 4- 300 K. The cryogenic temperature characteristics of the tested sensors are reported.

2. Coating thickness determination

Figure 1 shows the model of the dual layer metal recoated FBG sensors (DMCFBG) where material 2 serves as primary coating layer while material 1 severs as secondary coating layer. Figure 2 shows the cross section of the dual layer metal recoated FBG sensor.

To determine the coating thickness, the thermal stresses acting in the bare fiber and the coatings should be known. These stresses can be calculated by analyzing a simple theoretical model of FBG sensor shown in figure 2.In figure 2, r_0 = radius of core, r_1 = radius of the primary material coating (C_1),r_2 = radius of the secondary material coating (C_2),C_1 = Primary coating material,C_2 = Secondary coating material,P_1 = Lateral Pressure at the glass fiber and primary coating interface,P_2 = Lateral pressure at the primary coating and secondary coating interface. Following assumption are made to carry out this analysis.

- The optical fiber is infinite along the axial direction.
- There is no stress in the system at the initial temperature (i.e., the temperature at which the metallic coating is applied). The physical properties like Young’s modulus and coefficient of thermal expansion (TEC)) of glass fiber and metals are different. When there is difference between the operating temperature and coating application temperature, a stress is developed.
- Geometry of the DMCFBG sensor is symmetric along the axial direction (see figure 2).
- The FBG and recoating metals are isotropic materials.

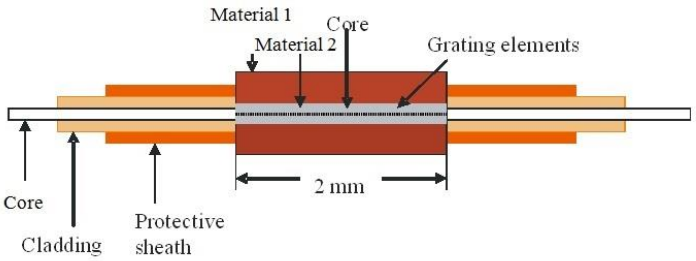

Figure 1. Dual layer metal coated FBG sensor (DMCFBG)

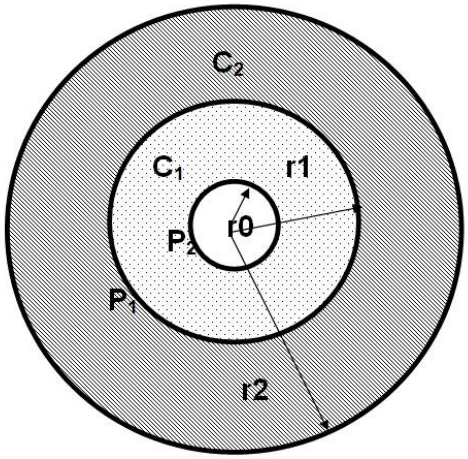

Figure 2. Model DMCFBG

2.1 Calculation of lateral pressure p_1 and p_2

The geometry about the axial direction of the DMCFBG sensor is symmetric as shown in figure 2. Hence a cylindrical co-ordinate system can be adopted. The stress-strain in cylindrical co-ordinate system can be expressed as [18],

$$\varepsilon_0 = -\alpha\,\Delta T(1+\nu) + \frac{1-\nu^2}{E}\left(\sigma_\theta - \frac{\nu}{1-\nu}\sigma_r\right) \tag{1}$$

Where σ_r, σ_θ , ε_θ, E, α, and ν are the radial stress, tangential stress, tangential strain, Young's modulus, coefficient of thermal expansion and Poisson's ratio of the material, respectively. The ΔT is the difference between the application temperature and operating temperature and it can be a positive or negative quantity. To find the various stresses, a model of thick walled tube with inner radii 'a' and the outer radii 'b' can be assumed. Using Lame formula [19], the stress components, at radius r in a circular thick walled tube subjected to internal pressure (p_i) and external pressure (p_e) can be expressed as [19].

$$\sigma_r = \frac{a^2b^2(p_e-p_i)}{(b^2-a^2)r^2} + \frac{p_ia^2-p_eb^2}{b^2-a^2}; \qquad \sigma_\theta = -\frac{a^2b^2(p_e-p_i)}{(b^2-a^2)\,r^2} + \frac{p_ia^2-p_eb^2}{b^2-a^2} \tag{2}$$

Substituting equation (2) in (1), radial displacement (u) can be obtained

$$u = r\varepsilon_0 = -\alpha\,\Delta T(1+\nu)\,r + \frac{(1+\nu)}{E}\frac{1}{(1-\gamma^2)} * \left[(1-2\nu)(\gamma^2 p_i - p_e)\,r - (p_e-p_i)\frac{a^2}{r}\right] \tag{3}$$

Where $\gamma = a/b$

Using Equation (3), radial displacement of the boundary of glass fiber (u_{01}) and the radial displacement of the inner boundary of primary coating (u_{11})can be reduced to,

$$u_{01} = -\alpha_0\Delta T(1+\nu_0)r_0 - \frac{1+\nu_0}{E_0}(1-2\nu_0)p_1r_0 \tag{4}$$

$$u_{11} = -\alpha_1\Delta T(1+\nu_1)r_0 + \frac{1+\nu_1}{E_1}\frac{1}{1-\gamma_1^2} * \left[(1-2\nu_1)(\gamma_1^2 p_1 - p_2) - (p_2-p_1)\right]r_0 \tag{5}$$

Here r_0 is the radius of the glass fiber, E_0 and ν_0 are elastic constants of the glass material, α_0 is its co-efficient of thermal expansion, u_{01} is the boundary of glass fiber,u_{11} is the inner boundary of primary coating,E_1 and ν_1 are elastic constants of the coating material**,** and

$$\gamma_1 = r_0 / r_1 \tag{6}$$

The radial displacement of the outer boundary of primary coating (u_{12}) and the radial displacement of the inner boundary of secondary coating (u_{22}) are

$$u_{12} = -\alpha_1 \Delta T(1+\nu_1) r_1 + \frac{1+\nu_1}{E_1}\frac{1}{1-\gamma_1^2} * \left[(1-2\nu_1)\left(\gamma_1^2 p_1 - p_2\right) - \left(p_2 - p_1\right)\right] r_1 \tag{7}$$

$$u_{22} = -\alpha_2 \Delta T(1+\nu_2) r_1 + \frac{1+\nu_2}{E_2}\frac{1}{1-\gamma_2^2} * \left\{\left[(1-2\nu_2)\gamma_2^2 + 1\right] p_2\right\} r_1 \tag{8}$$

$$\gamma_2 = r_1 / r_2 \tag{9}$$

$\alpha_1(T)$ is the actual ("instantaneous") co efficient of thermal expansion, T_0 is the application ("zero –stress") temperature of the coating material, ΔT is the change in temperature, and p is the interfacial pressure caused by the thermal contraction mismatch of the materials. The first terms in equations (4), (5), (7), and (8) are due to unrestricted thermal contractions, and the second terms are due to the interfacial pressure p. For meeting compatibilities of displacements requirements, following condition have to be satisfied:

$$u_{01} = u_{11} \;;\; u_{12} = u_{22} \tag{10}$$

Based on (10), following expressions are derived for lateral pressure calculation.

$$P_1 = E_1\alpha_1\Delta T \frac{\dfrac{E_1}{E_2}\dfrac{(1-2\nu_2\gamma_2^2+\gamma_2^2)}{1-\gamma_2^2} - \dfrac{1+\nu_1}{1+\nu_2} + \dfrac{2\alpha_2}{\alpha_1}\dfrac{1-\nu_1}{1-\gamma_1^2}}{\dfrac{(1+\nu_1)(1-2\nu_1)}{1+\nu_2} + \dfrac{E_1}{E_2}\dfrac{(1-2\nu_1\gamma_1^2+\gamma_1^2)(1-2\nu_2\gamma_2^2+\gamma_2^2)}{(1-\gamma_1^2)(1-\gamma_2^2)}} \tag{11}$$

$$P_2 = E_1\alpha_1\Delta T \frac{\dfrac{\alpha_2}{\alpha_1}\dfrac{(1-2\nu_1\gamma_1^2+\gamma_1^2)}{1-\gamma_1^2} - \dfrac{1+\nu_1}{1+\nu_2}}{\dfrac{(1+\nu_1)(1-2\nu_1)}{1+\nu_2} + \dfrac{E_1}{E_2}\dfrac{(1-2\nu_1\gamma_1^2+\gamma_1^2)(1-2\nu_2\gamma_2^2+\gamma_2^2)}{(1-\gamma_1^2)(1-\gamma_2^2)}} \tag{12}$$

Where P_1 is the lateral pressure at the interface of primary coating and the glass fiber, and P_2 is the lateral pressure at the interface of the primary coating and the secondary coating.

2.2 Calculation of Normal Stresses

The radial stress σ_r and tangential stress σ_θ in a glass fiber are simply equal to the negative pressure p_1,

$$\sigma_r = \sigma_\theta = -p_1 \tag{13}$$

The radial and the tangential stresses in the primary coating can be obtained from equation (14) and (15). By setting $p_i = p_1$, $p_e = p_2$, $a = r_o$, and $b = r_1$ in the expression for σ_r and σ_θ, gives

$$\sigma_r = \frac{r_0^{\,2} r_1^{\,2}(p_2 - p_1)}{\left(r_1^{\,2} - r_0^{\,2}\right) r^2} + \frac{p_1 r_0^{\,2} - p_2 r_1^{\,2}}{r_1^{\,2} - r_0^{\,2}} \quad for\, r_0 \le r \le r_1 \tag{14}$$

$$\sigma_\theta = -\frac{r_0^{\,2} r_1^{\,2}(p_2 - p_1)}{\left(r_1^{\,2} - r_0^{\,2}\right) r^2} + \frac{p_1 r_0^{\,2} - p_2 r_1^{\,2}}{r_1^{\,2} - r_0^{2}} \quad for\, r_0 \le r \le r_1 \tag{15}$$

Similarly σ_r and σ_θ in the secondary coating can be obtained from equation (16) and (17) by setting
$p_i = p_2$, $p_e = 0$, $a = r_1$, and $b = r_2$.

$$\sigma_r = p_2 \frac{\left(r^2 - r_2^2\right) r_1^2}{(r_3^2 - r_2^2) r^2} \quad for\ r_1 \le r \le r_2 \tag{16}$$

$$\sigma_\theta = p_2 \frac{\left(r^2 + r_2^2\right) r_1^2}{(r_3^2 - r_2^2) r^2} \quad for\ r_1 \le r \le r_2 \tag{17}$$

The axial stress, σ_Z is given by

$$\sigma_z = v\left(\sigma_r + \sigma_\theta\right) + E\,\alpha\,\Delta T \tag{18}$$

Hence, the axial stresses in the glass fiber, primary coating, and secondary coating are

$$\sigma_z = -2vp_1 + E_0\,\alpha_0\,\Delta T \quad for\, r \le r_0 \tag{19}$$

$$\sigma_z = -2v_1 \frac{p_1 r_0^2 - p_2 r_1^2}{r_1^2 - r_0^2} + E_1\,\alpha_1\,\Delta T \quad for\, r_0 \le r \le r_1 \tag{20}$$

$$\sigma_z = 2v_2 p_2 \frac{r_1^2}{r_2^2 - r_1^2} + E_2\,\alpha_2\,\Delta T \quad for\, r_1 \le r \le r_2 \tag{21}$$

Using equation ((18) - (21)), the effect of increase in thickness of the primary and the secondary coating layers of the DMCFBG sensor can be found. It is evident from expressions 19, 20 and 21 the coating thickness plays a vital role in determining stress acting on the fibers. Hence it is important to carry out the system study of the effect of this parameter on the stress generation.

Figure 3(a) and 3 (b) shows the variation of the radial, tangential and axial stress corresponding to the primary coating thickness. The superscripts a, b, c and d in the following graphs denote the stresses at the inner boundary of the primary coating layer, outer boundary of the primary coating layer, inner boundary of the secondary coating layer and outer boundary of the secondary coating layer respectively. Table 1 and 2 summarizes radial, tangential and axial stresses acting on the fiber due to the increasing thickness of the primary and secondary metallic coating layer respectively.

From figure 3(a), it can be seen that the increase in the primary coating increases the stress developed in primary coating which in turn gets transferred to the glass fiber. But the increase in stress value is more at lower thickness. As the thickness increases to a value more than 125 microns, the increase in the stress rate is very small. Considering this, the thickness for the primary coating is chosen as 125 micron in the sensor fabrication. Aluminium is considered for primary coating, which can be easily deposited on a glass fiber using Al vaporization method. Figure 3(b) shows that the secondary coating thickness of 625 microns can be chosen as stress level reaches its saturation value after this thickness. Beyond this value of thickness the measurement speed will be affected and the sensor system will be bulky. The materials considered in this present work for the secondary coatings are indium, lead, and copper.

Table 1 Effect of increasing the primary coating layer material thickness

Parameter & Stresses		Effect of increasing the primary coating layer material parameter			
		IBPL	OBPL	IBSL	OBSL
Increase of Coating Thickness	Radial	Increase	Increase	Increase	Zero
	Tangential	Increase	Increase	Decrease	Decrease
	Axial	Increase	Increase	Decrease	Decrease

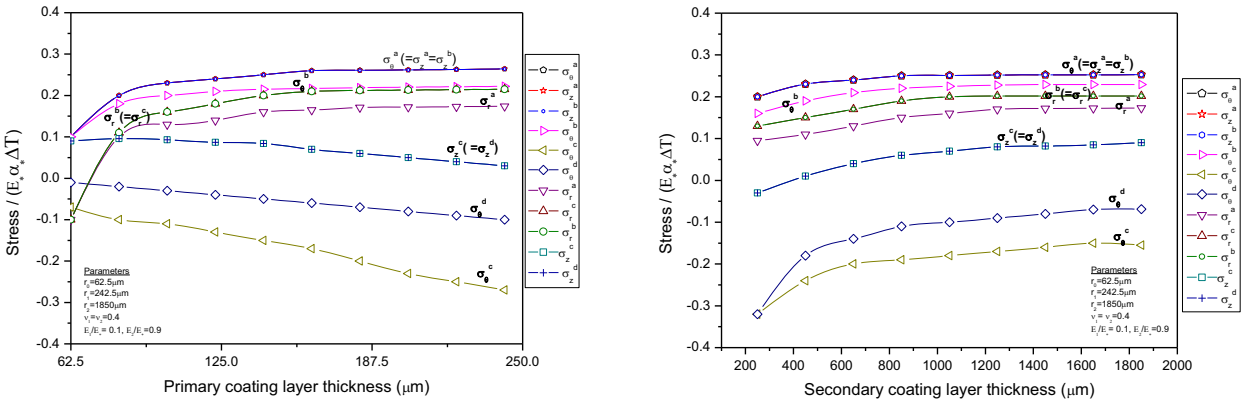

Figure 3(a) and 3(b). Stress variations for primary coating and secondary layer thickness

Table 2 Effect of increasing the secondary coating layer material thickness

Parameter & Stresses		Effect of increasing the secondary coating layer material parameter			
		IBPL	OBPL	IBSL	OBSL
Increase of Coating Thickness	Radial	Increase	Increase	Increase	Zero
	Tangential	Increase	Increase	Increase	Increase
	Axial	Increase	Increase	Increase	Increase

IBPL = Inner boundary of the primary layer, OBPL = Outer boundary of the secondary layer
IBSL= Inner boundary of the secondary layer, OBSL = Outer boundary of the secondary layer

3. Experiment and results

The sensors were fabricated with determined thicknesses of dual metals. An Experimental setup to study the temperature response metal recoated FBG sensors (FBG sensors recoated with aluminium, copper, lead and indium) was constructed. All metal recoated FBG sensors have thin aluminium recoating as a primary layer. The temperature measurements of these sensors are carried out keeping the strain constant. For this purpose the sensors are left to be hanging freely inside the cryostat. This ensures that FBG sensor response is only due to the thermal stress acting on the grating element. The cryostat is cooled down to 4.2 K from 300 K by supplying liquid nitrogen (LN_2 ~ 77 K) and liquid helium (LHe ~ 4.2 K). The temperature is controlled by the heating elements in the calibration block controlled by the computer. The response of the reference sensors (TVO) and the FBG sensors are recorded in a dedicated

Laptop using LabVIEW 8.2 program. The metals like aluminium, copper, lead and indium are used for recoating the FBG sensor and these sensors were tested at low temperature range of 300 K – 4.2 K. Figure 4, show the thermal response of the Al-Al DMCFBG, Al-Cu DMCFBG, Al-Pb DMCFBG sensors, and Al-In DMCFBG sensors. Figure 5 shows sensitivity comparison bar chart of DMCFBG sensor at the temperatures of 50 K , 20 K and at 15K. From the chart it can be observed that the sensitivity for the indium and lead coated FBG sensors is high when compared to polymer and other DMCFBG sensors. Also, the sensitivity of indium and lead DMCFBG sensors are close to each other.

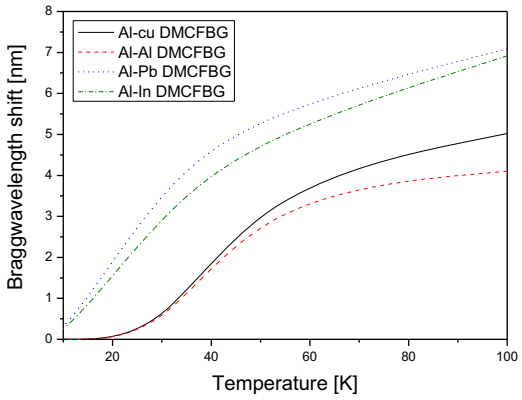

Figure 4 Comparison DMCFBG sensors.

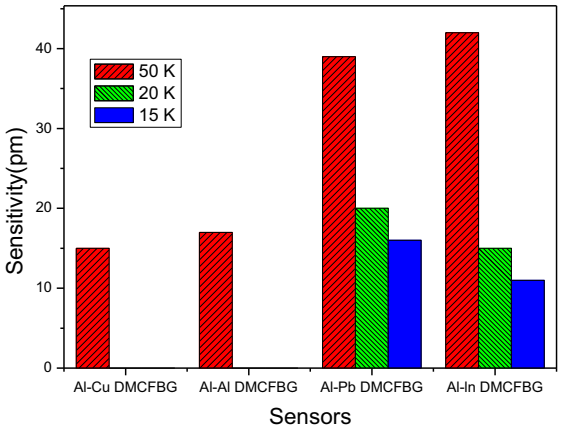

Figure 5 Sensitivity of DMCFBG

4. Conclusion

In this work, different metal were considered for coating the FBG sensor. For theoretical investigation, a double layered circular thick wall tube model has been considered to study the effect on sensitivity due to the mechanical properties like Young`s modulus, Thermal expansion coefficient, Poisson's ratio of selected materials at a various cryogenic temperatures. The primary and the secondary coating thickness for a dual layer metal coated FBG sensor have been determined to be 125 µm and 625 µm from the above study. The sensor was then fabricated and tested at cryogenic temperature range from 4-300 K. The cryogenic temperature characteristics of the tested sensors are reported. The results show that lead and indium coated DMCFBG sensors show greater sensitivity upto 20 K while indium coated DMCFBG sensors show greater sensitivity at lower temperature range of 50K- 4.2K. The sensitivity in this temperature range is found to be 0.022 nm /K for lead and 0.028 nm / K for indium. The sensors are found to be reasonably sensitive to a low temperature of 15 K.

.

5. References

[1] Inaudi D, Glisic B, Scandale W, Garcia Perez J, Billan J, Radaelli S 2001, *Proc. SPIE **4328***. 79-87
[2] Fernandez A F, Brichard B, Borgermans P, Berghmans F, Decreton M, Megret P, Blondel M, Delchambre A 2002 *Optical Fiber Sensors Conference Technical Digest,* **Vol.1**. 63-66
[3] Ramalingam R, Suesser M,Neumann H 2009 *Proceedings OPTO 2009 & IRS² 2009.* 113-118.
[4] K. Iniewski 2013 *Smart Sensors for Industrial Applications* (Lengmuir:CRC Press)
[5] Hill K O, Fujii Y, Johnson D C, Kawasaki B S 1978 Appl. Phys. Lett., 1978, **32** 647-9.
[6] Hill K O, Meltz G 1997 Journal of Lightwave Technology **15** 1263-76.
[7] Kashyap R 1999 Fiber Bragg Gratings (Academic Press: San Diego)
[8] Bharathwaj V, Markan A, Atrey M, Neumann H, Ramalingam R 2014 *Sensor,IEEE* **14834053** 1535-38
[9] Ramalingam R, Neumann H 2011 *Sensors Journal, IEEE* **11** 1095-1100.

[10] Ramalingam R, Nast R, Neumann H 2015 *Sensors Journal, IEEE* **15** 2023- 30.
[11] Ramalingam R, Kläser M, Schneider T, Neumann H 2014 *Sensors Journal, IEEE* **14** 873- 81
[12] Jicheng L, Neumann H, Ramalingam R 2015 *Cryogenics* **68** 36-43.
[13] Ramalingam R 2012 *Proceedings of ICEC 24-ICMC 2012* 43-46
[14] Ecke W, Latka I, Habisreuther T, Lingertat J 2007 *Proc. SPIE **6530*** 653002
[15] Xue L, Liu J, Liu Y, Jin L, Gao S, Dong B, Zhao Q, Dong X 2006 Applied Optics **45** 8132-35
[16] Lupi C, Felli F, Brotzu A, Caponero M A, Paolozzi A 2008 *IEEE Sensors Journal* **8** 1299-1304
[17] Szocs E, Schwager F, Toben M, Brese N 2008 *Proceedings of 2nd Electronics System-Integration Technology Conference* 347-350.
[18] Timoshenko, S. P. and Goodier J N, Theory of Elasticity, 3rd Ed. McGraw-Hill, 1970 New York, NY, U.S.A.
[19] Laurson and Cox., “Mechanics of Materials" 2nd edition 1938 Wiley and Sons.